applied sciences

MDPI

Article

Effect of Characteristics of Ground Motion on Seismically Induced Sliding Surface of Slopes

Muhammad Irslan Khalid [1], Yonggook Lee [1], Yonghee Lee [2], Hak-Sung Kim [2] and Duhee Park [1,*]

[1] Department of Civil and Environmental Engineering, Hanyang University, Seoul 04763, Korea; engrarslan_civil@outlook.com (M.I.K.); dwcollector@hanyang.ac.kr (Y.L.)
[2] Central Research Institute, Korean Hydro and Nuclear Power Corporation, Daejeon 34101, Korea; dragon202@khnp.co.kr (Y.-H.L.); haksung.kim@khnp.co.kr (H.-S.K.)
* Correspondence: dpark@hanyang.ac.kr; Tel.: +82-2-2220-0322

Abstract: The seismic performance of slopes is typically evaluated with a pseudo-static method using equivalent horizontal load or with Newmark sliding block analysis. In both procedures, the definition of the potential sliding surface is a required input. The sliding surface has been reported to be marginally influenced by the input ground motion and, therefore, is most often assumed from a pseudo-static procedure. In this study, extensive series of two-dimensional dynamic nonlinear finite element analyses are performed to evaluate the sensitivity of the sliding surface on the slope geometry, soil strength parameters, and input ground motion characteristics. It is demonstrated that the sliding surface may vary with the intensity and frequency characteristics of the input motion. Slopes with inclination angle equal or less than 35° are shown to be marginally influenced by motion intensity if the mean period (T_m) < 0.3 s. However, slopes inclined at 45° are revealed to be more sensitive to the motion intensity and T_m. For motions with T_m > 0.3 s, the sliding surface is demonstrated to widen with an increase in the intensity of the input ground motions. The degree of widening increases proportionally with an increase in T_m. It is, therefore, recommended to derive sliding surfaces from a dynamic analysis for steep slopes.

Keywords: seismic slope stability; sliding surface; finite element; dynamic analysis; nonlinear soil model

Citation: Khalid, M.I.; Lee, Y.; Lee, Y.-H.; Kim, H.-S.; Park, D. Effect of Characteristics of Ground Motion on Seismically Induced Sliding Surface of Slopes. *Appl. Sci.* **2021**, *11*, 5319. https://doi.org/10.3390/app11125319

Academic Editor: Andrea Paglietti

Received: 28 April 2021
Accepted: 4 June 2021
Published: 8 June 2021

1. Introduction

Catastrophic hazards produced by seismically induced slope failures have been widely observed in previous severe earthquakes [1,2]. Therefore, a reliable prediction of the seismic performance of slopes is essential. Assessing the stability of the slope has been a difficult task for engineers because the factors controlling the dynamic response and failure mechanism of the slope are not yet fully understood.

A wide range of approaches is available to predict the seismic stability of the natural and engineered slopes (e.g., dams and embankments). These include (a) pseudo-static method; (b) Newmark sliding block method; (c) stress deformation methods. The pseudo-static approach is the simplest and most widely used design method for the calculation of the factor of safety [3–5]. The pseudo-static method is recommended in many codes and design guidelines for conventional projects. However, the pseudo-static approach has been reported to have inherent drawbacks, which include the assumption of a rigid perfectly plastic behavior of soil and uncertainty in approximating the transient nature of earthquake loading as an equivalent force utilizing a horizontal seismic coefficient, k, which represents the lateral acceleration normalized by the gravitational acceleration. The second most practiced design concept was presented by Newmark [6], which is termed as the Newmark sliding block model. In this method, the soil mass above the failure surface is assumed as a rigid block, which slides and produces a permanent displacement when yield acceleration (k_y) is exceeded. Many researchers have used the Newmark sliding block

concept to calculate permanent downslope displacements. New equations and empirical charts were proposed to account for the effect of ground motion characteristics. Jibson [7,8] proposed a regression model to estimate landslide displacement based on strong motion records. However, the model is only recommended for preliminary screening or regional scale hazard mapping. Saygili and Rathje [9] developed an empirical predictive model for predicting the earthquake induced displacements based on the Newmark sliding block procedure. In these studies, the soil mass was assumed as a rigid block. Rathje and Antonakos [10] developed a unified predictive model to account for dynamic response of sliding mass. Tsai and Chien [11] followed the same hypothesis and developed a displacement model for rigid and flexible slopes. In both pseudo-static and Newmark methods, it has been assumed that the critical sliding surface is independent on the frequency characteristics and amplitude of the input ground motion. The surface determined from a limit equilibrium analysis has been utilized.

The dynamic analysis method has been used as an alternative procedure to evaluate the seismic performance of slopes [12–14]. However, it should be noted that a majority of the studies still use the Newmark sliding block framework to extract the Newmark displacement. In this procedure, the stresses acting on a predefined failure surface are integrated to determine equivalent acceleration time history along the surface. It is used along with k_y to determine the Newmark displacement. Therefore, in a dynamic analysis, the definition of a predefined failure surface is necessary. Lee et al. [15] performed a series of finite difference (FD) analysis to calculate the earthquake-induced displacements in mountain slopes. The sliding surfaces calculated from the limit equilibrium and FD analyses were revealed to be similar. It should be noted that the slopes considered were composed of thin soil layer over inclined bedrock, for which the variability of the sliding surface is constrained because of the limited depth of the layer. Tsai and Lin [16] performed two-dimensional (2D) equivalent linear dynamic analyses to predict the slope displacement considering shallow, medium, and deep sliding planes calculated from limit equilibrium analyses. Fotopoulou and Pitilakis [17] performed 2D finite element (FE) analyses to develop a new empirical model for slope displacement. The sliding surface was calculated by the Bishop's simplified method. Cho and Rathje [18] performed non-linear FE analyses to develop the predictive model for the earthquake-induced slope displacements. The sliding surface determined from the FE analysis was reported to be similar to that characterized from a parallel limit equilibrium analysis. However, only a single case was presented. Comprehensive comparisons for various slopes and input ground motions were not provided. The literature review highlights that, in pseudo-static, Newmark sliding block, and even dynamic analyses, the sliding surface is most often determined from the limit equilibrium method. The effect of the input ground motion on the sliding surface has not yet been extensively evaluated.

The purpose of this study is to evaluate the sensitivity of the sliding surface on the slope geometry, soil parameters, and input motion characteristics. An extensive series of 2D nonlinear FE analyses was performed. The sliding surface was determined from the maximum shear strain contour at the end of shaking. The sliding surfaces derived in this study are compared with those determined from the parallel limit equilibrium-based procedure. The differences between the surfaces are quantified. The result of this study is expected to have an influence on the procedure of determining the Newmark displacement from a dynamic analysis.

2. Material and Methods

2D dynamic nonlinear analyses were performed using the commercial FE program LS-DYNA (2D) [19] to simulate the non-linear response of slope, as shown in Figure 1. The program uses the explicit central difference time integration scheme in solving the dynamic equation of motion. The semi-discrete equation of motion at time n is shown in

Equation (1). Where diagonal mass matrix is represented by M, external and body force load is accounted as P^n, stress divergence vector as F^n and hourglass resistance as H^n [19].

$$Ma^n = P^n - F^n + H^n \quad (1)$$

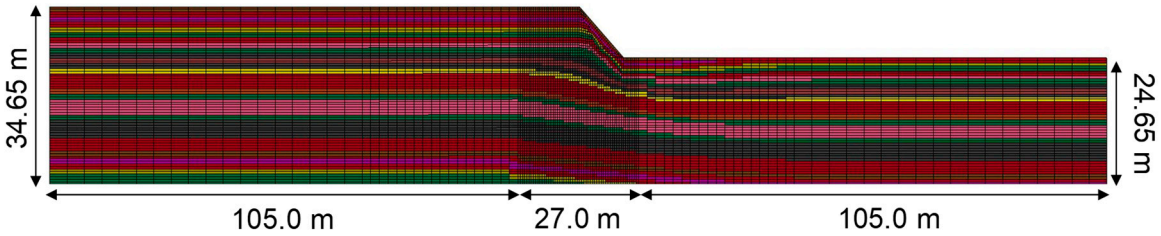

Figure 1. Numerical model of the slope.

The dimensions of the numerical model were 10 m slope height, 27 m wide, and 34.65 m in depth. For simulation of the rigid base, a prescribed motion boundary condition was assigned to the base nodes of the slopes. Due to the difference in the height of vertical edges of the soil domain, the equal degree of freedom (EDOF) constraint was not applied. Instead, the lateral boundaries were fixed in the horizontal direction. A sensitivity study was performed to select the extent of lateral boundaries, such that they do not influence the response of the slopes due to the reflected waves. Conservatively, the distance from the slope to both ends of the lateral boundaries was set to 105 m.

The soil domain was discretized using four noded-plane strain elements. The size of the smallest element was selected such that the maximum wave frequency (f_{max}) is higher than 25 Hz as recommended for the site response analysis [20,21]. f_{max} was calculated as $f_{max} = Vs/4h$, where h is the height of the element and Vs is the shear wave velocity. The element size selected was 0.5 m, which is also smaller than recommended by Kuhlemeyer and Lysmer [22]. The slope area was discretized using a fine mesh. The mesh size gradually increases towards the lateral boundary to reduce the computational cost without affecting the numerical accuracy. In the computational model, slope was discretized into layers such that, within each layer, the confining pressure is within a narrow range. Therefore, inclined layers were used for the slope, as shown in Figure 1. This type of discretization was necessary because Vs is influenced by the confining pressure.

The nested-yield surface plasticity model implemented in LS DYNA was used to simulate the nonlinear behavior of soil (MAT_HYSTERETIC model). The non-linear shear stiffness is represented in a piecewise manner by separating the shear behavior across multiple linear elastic perfectly plastic yield surfaces. The elastic stiffness and size of the yield surfaces are controlled by a backbone curve of the shear stress versus shear strain at a reference pressure. Modulus degradation and Masing rule damping are determined internally based on the user-defined stress–strain inputs. The value of stress at any instant is equal to the sum of the stresses in the individual elastic-perfect plastic layers, which results in a piecewise backbone curve. It has been widely used for seismic site response analyses [21,23,24]. The properties are pressure dependent on descrambling by the following equations [19]:

$$G(p) = \frac{G_0(p - p_0)^b}{(p_{ref} - p_0)^b} \quad (2)$$

$$\frac{\tau(p)}{\tau\left(p_{ref}\right)} = \sqrt{\frac{a_0 + a_1(p - p_0) + a_2(p - p_0)^2}{a_0 + a_1\left(p_{ref} - p_0\right) + a_2(p_{ref} - p_0)^2}} \quad (3)$$

where p is the current pressure, p_o is the cut-off or datum pressure, p_{ref} is the reference pressure at which input value are calculated, G_o is the shear modulus of the layer at the reference pressure, G(p) is the shear modulus of the layer at pressure p, $\tau(p_{ref})$ is the

yield stress of the layer at the reference pressure, $\tau(p)$ is the yield stress of the layers at pressure p, b is the exponent for pressure sensitive moduli and a_0, a_1 and a_2 are the yield function constants.

The pressure-dependent shear modulus reduction curves were developed for each layer using Darendeli [25] formulation. The shear strength correction was applied by a generalized quadratic/hyperbolic (GQ/H) constitutive model [26], in which the shear stress–strain curve follows a shear modulus reduction curve up to a shear strain of approximately 0.1% and then at large strains, it achieves the target shear strength. The shear strength of the soil was calculated using the Mohr–Coulomb failure criterion.

LS-DYNA utilizes the input shear stress–strain curve to calculate the modulus reduction and soil damping using the Masing rule [27]. Each layer was assigned the stress–strain curve based on the value of the *Vs* and confining pressure. Figure 2 shows the modulus reduction and damping curves calculated at various depths. Additionally, shown are the target Darendeli nonlinear curves plotted for comparison purposes.

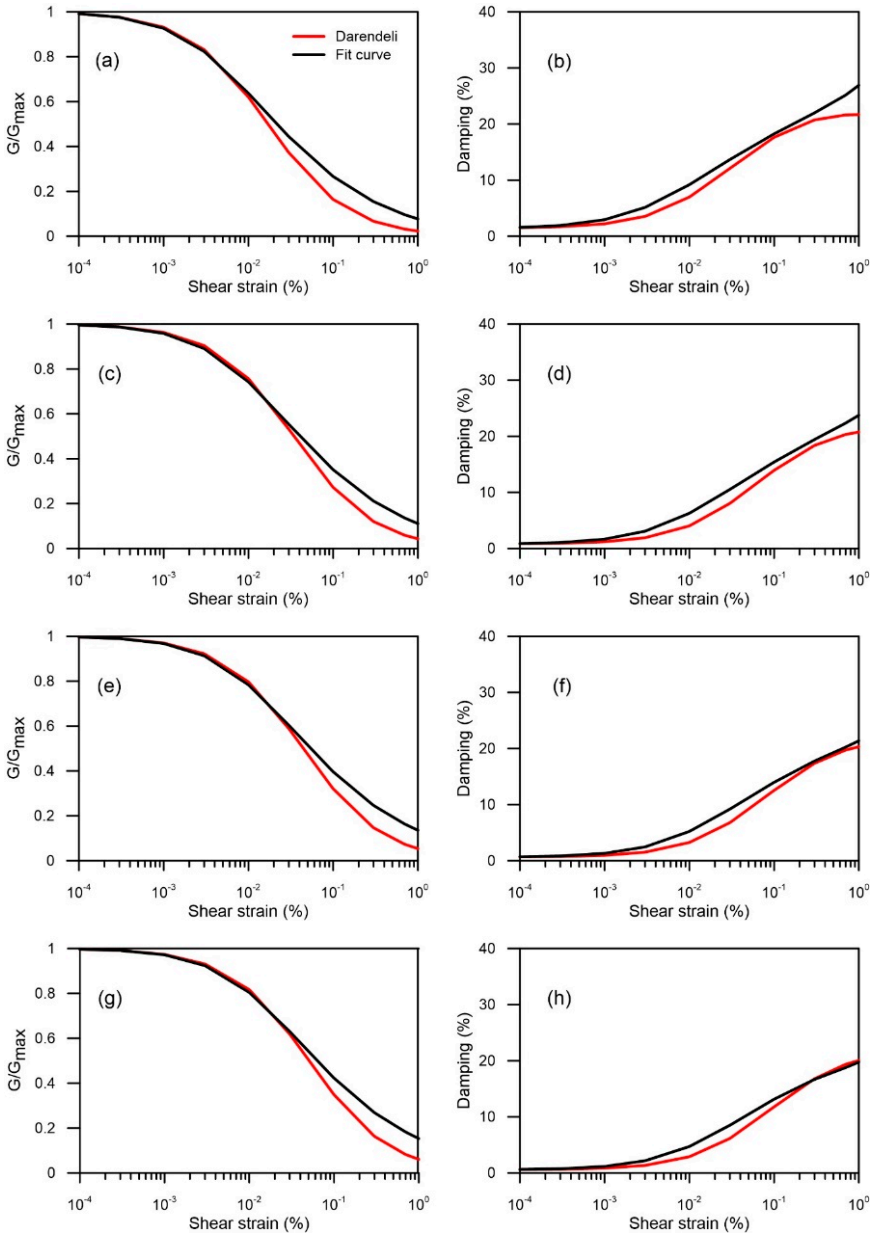

Figure 2. Modulus reduction and damping versus strains curves (**a**,**b**) 2.0 m (**c**,**d**) 10.0 m (**e**,**f**) 20.0 m (**g**,**h**) 30.0 m.

A frequency-independent formulation was used to model the small strain damping using the damping frequency range option. Darendeli [25] curves were used to select the soil layers small strain damping. The range of the highest and lowest frequencies for the small-strain damping was recommended as 30.0 Hz and 0.1 Hz, respectively [21]. The numerical analysis consisted of a static analysis to establish the gravitational stress field, followed by a dynamic analysis using input ground motion. The numerical model was thoroughly validated against centrifuge model tests, the details of which are reported in Lee et al. [28].

3. Parametric Study

A parametric study was performed to evaluate the influence of the input motion, slope geometry and soil properties. The matrix of the dynamic analyses performed for the parametric analysis is summarized in Table 1. A total of twelve slope models were used. Three slope angles were used, which are 25°, 35°, and 45°. Two friction angles (ϕ') were used, which are 30° and 40°. Two cohesion values were assigned, which are 6 kPa and 12 kPa. The V_S profile was generated using the following empirical correlation:

$$Vs = 57.372\ {\sigma_c}^{0.2751} \quad (4)$$

where Vs is shear wave velocity (m/s) and σ_c is the confining pressure (kPa). The equation was developed from the results of a series of resonant column test using silty sand specimens. The calculated shear wave velocity from the empirical relationship are in line with the typical range for granular soil, as reported in Yoo et al. [29]. Vs was not correlated with the shear strength because the unavailability of the strength and confining pressure dependent correlation to estimate Vs. Additionally, the influence of Vs on the failure surface is estimated to be marginal. The shear modulus was calculated from Vs, where the density was set to 1.784 g/cm^3. The Poisson's ratio was set to 0.30.

Table 1. Summary of the cases performed.

Case	Slope Angle (°)	Friction Angle (ϕ') (°)	Cohesion (c') (kPa)	Static Factor of Safety
1	25	30	6	1.8
2			12	2.2
3		40	6	2.5
4			12	2.9
5	35	30	6	1.4
6			12	1.7
7		40	6	1.8
8			12	2.1
9	45	30	6	1.1
10			12	1.4
11		40	6	1.4
12			12	1.7

Among twelve slope models, the baseline characterization is Case 9.

Four recorded ground motions were used, as listed in Table 2. The baseline corrected motions were amplitude scaled to four peak ground accelerations (PGAs), which are 0.25 g, 0.50 g, 0.75 g, and 1.0 g, resulting in sixteen motions. The acceleration time history and response spectra of these motions scaled to PGA = 0.25 g are shown in Figure 3. Table 2 lists the characteristics of the input ground motions. The motions are listed in the order of mean period (T_m).

Table 2. Characteristics of input ground motions selected for dynamic analyses.

Earthquake	PGA (g)	Predominant Period (s)	Mean Period (s)
Whittier Narrows	0.188	0.156	0.159
Northridge	0.221	0.20	0.250
Ofunato	0.186	0.195	0.317
Kobe	0.25	0.34	0.646

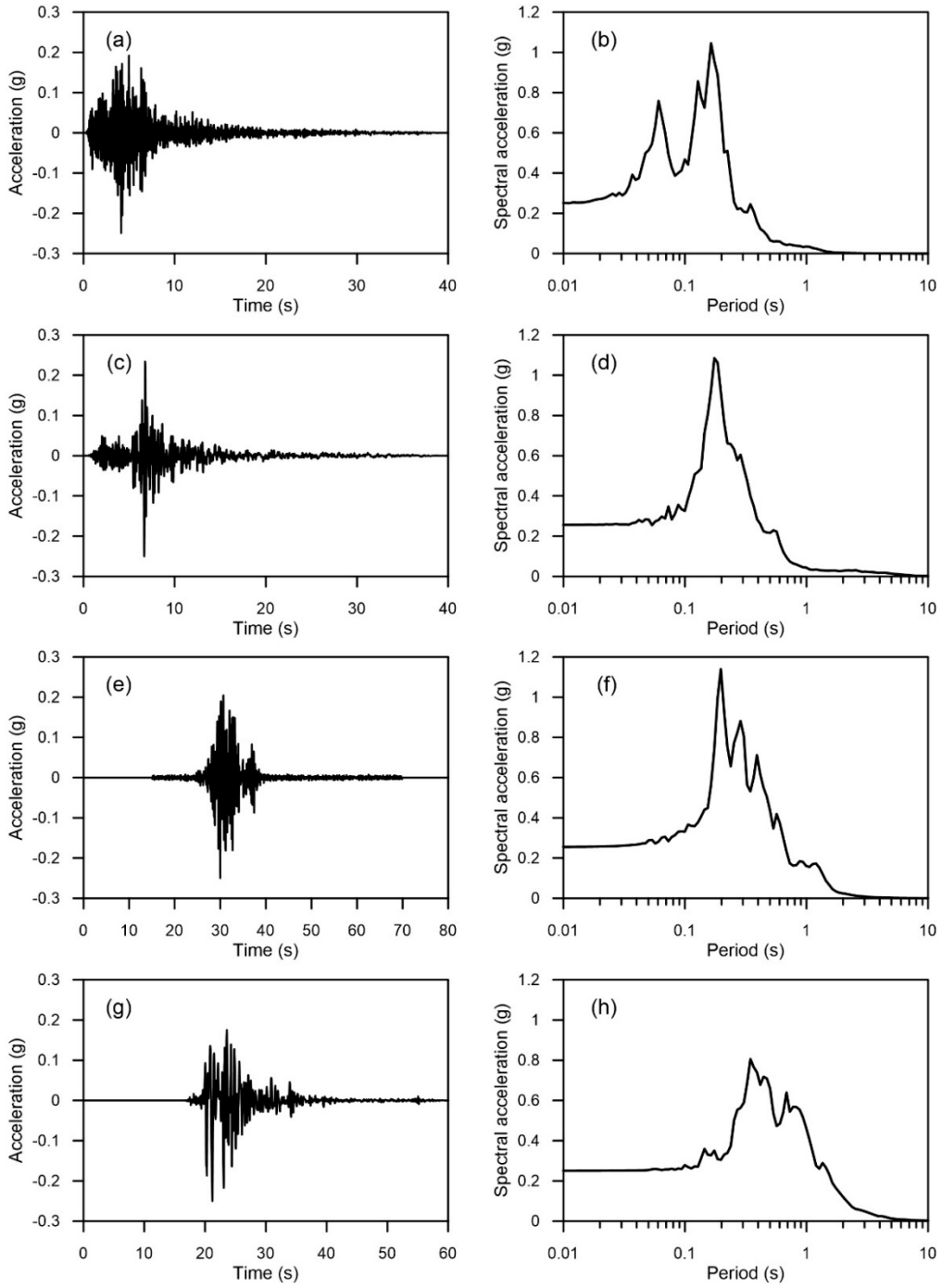

Figure 3. Acceleration time histories and 5% damped response spectra of earthquake ground motions used in the analyses (**a**,**b**) Whittier Narrows (**c**,**d**) Northridge (**e**,**f**) Ofunato (**g**,**h**) Kobe.

4. Results

4.1. Failure Surfaces Determined from Pseudo-Static Analyses

For comparison purposes, the critical slip surfaces were calculated from pseudo-static analyses. They were calculated with the Morgenstern–Price method using the commercial software Slope/w [30]. The surfaces were calculated for zero horizontal load and equivalent loads that result from PGA = 0.25, 0.5, 0.75 and 1.0 g.

A comparison of the effect of soil properties on the failure surface for static condition for the uniform slope inclined at an angle of 45° is depicted in Figures 4 and 5. Figure 4 shows the friction angle effect on the failure surface for a fixed cohesion value of 6 kPa. The results show that the failure surfaces shape is not highly affected by the soil friction angle. Similar trends are observed for other values of cohesions and slope angles. Figure 5 presents the change in the shape of failure surface with a variation of soil cohesion value for $\phi' = 30°$. As the cohesion increases, the static failure surface becomes deeper.

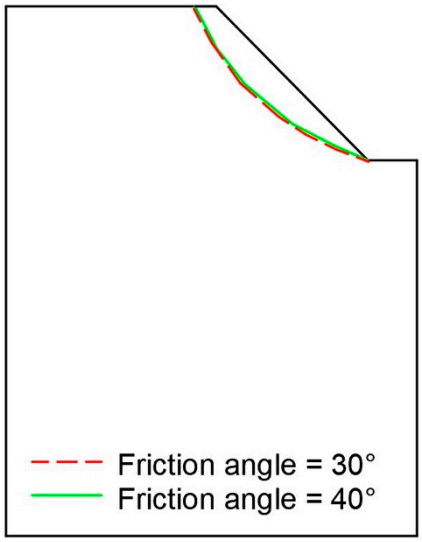

Figure 4. Effect of friction angel on static failure surface for cohesion value of 6 kPa.

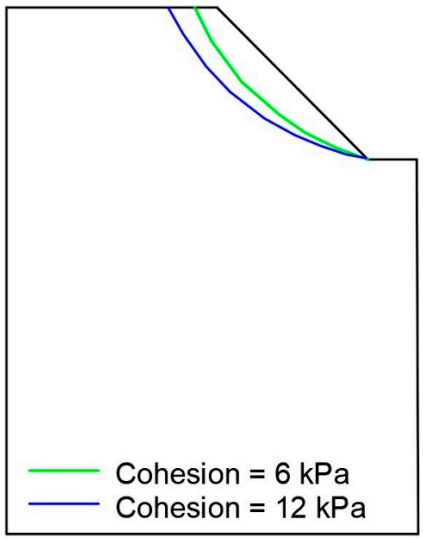

Figure 5. Effect of cohesion on static failure surface determined from limit equilibrium method.

Further analyses were performed to evaluate the influence of the equivalent lateral load on the failure surface. Figure 6 shows the failure surface calculated from the pseudo-static analyses. The failure surfaces are similar to the sliding surface determined from

a static analysis up to an amplitude of 0.50 g for the slope inclined at an angle of 45°. The failure surface is revealed to widen at higher PGAs. For other slope angles and soil properties, similar trends were observed. The pseudo-static analysis outputs demonstrate that the sliding surface may be influenced by the applied load at higher values of input static equivalent load. The failure surfaces were determined from pseudo-static analyses by applying equivalent lateral loads. They are compared with those derived from parallel dynamic analyses, the details of which are presented in the following section.

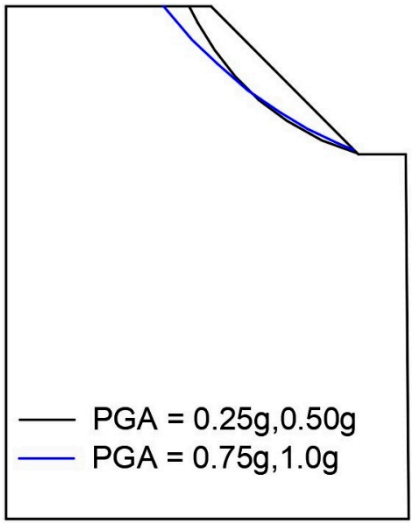

Figure 6. Effect of equivalent horizontal load on the sliding surface for c' = 6 kPa and ϕ' = 30°.

4.2. Failure Surfaces Determined from Dynamic Analyses

For dynamic analyses, the sliding surfaces were determined from the maximum shear strain contour at the end of the simulation. The depths at which maximum shear strain is induced along a series of selected vertical planes were recorded. The sliding surface was determined by connecting these marked depths. It should be noted that a level of smoothing was required at a number of cases in developing the sliding surface. This process of extracting the sliding surface is illustrated in Figure 7, which shows the maximum shear strain contours for the Case 11 using Ofunato motion scaled to PGA = 0.25 g. The points at which the maximum shear strains are produced along the selected vertical planes are shown as open circles. The estimated failure surface is shown as red line. Additionally, shown is the statically determined sliding surface. In this study, the residual between the sliding surfaces extracted from dynamic and pseudo-static analyses is quantified as the difference in the areas of the sliding masses calculated from respective methods in log normal unit.

4.3. Effect of Intensity of Ground Motion

In this section, the effects of the input ground motion intensity and frequency characteristics are evaluated. The baseline case (Case 09) was used in all simulations. Figure 8 shows the failure surfaces developed subjected to Whittier Narrows, Northridge, Ofunato, and Kobe motions scaled to four levels of PGAs. Figure 8 shows that the failure surfaces determined from dynamic analyses are different from those calculated from pseudo-static analyses. It can also be observed that the shapes of failure surface also depend on the type of input ground motion and its intensity. For the Whittier Narrows motion, the failure surfaces derived from the dynamic analyses display limited change in the shape with a variation in the intensity, whereas those produced from pseudo-static analyses widen with an increase in the intensity of input ground motion. The failure surfaces calculated from the dynamic analyses for PGA = 0.25 g and 0.5 g are wider compared to the pseudo-static analysis-based surfaces. However, they are almost identical for PGA = 0.75 g and 1.0 g. Similar trends are revealed for the Northridge motion. The discrepancy between the surfaces

generated from the dynamic and pseudo-static analyses increase with an increase in the T_m of the input ground motions. They show distinct deviations for both Ofunato and Kobe motions. For the Ofunato motion, the failure surfaces determined from dynamic analyses are relatively wider compared to those produced by the Whittier Narrows and Northridge motions up to PGA = 0.75 g, whereas the surface for PGA = 1.0 g is displayed to become significantly wider. It is possible that the longer T_m produces longer wavelengths and, therefore, generates wider failure surface. For the Kobe motion, which has the longest T_m, the widest failure surfaces are generated. Almost all planar surfaces are produced by Kobe motions. It is demonstrated that the pseudo-static analysis fails to capture the change in the failure surfaces produced by different motions. The close comparisons demonstrate that the failure surfaces are influenced by both the T_m and intensity of the input ground motion. It is not possible to identify and quantify the influence of the frequency characteristics and intensity of the input motions based on the limited number of motions and slope characterizations utilized in this study. However, based on the observations, it is revealed that the failure surface needs to be characterized from a dynamic analysis rather than a pseudo-static method.

4.4. Effect of Slope Angle and Soil Properties

The results presented in the previous section are calculated for the baseline characterizations (Case 9). The effect of the input ground motion may depend on the slope characterization, the parameters of which include the slope angle and soil strength parameters. The results of all simulations performed in this study are summarized in Figure 9. The difference between the surfaces determined from the dynamic and pseudo-static analyses are quantified with the residual, which is defined in the previous section. It should be noted that a positive residual means that the failure surface determined from the dynamic analysis is wider and the mobilized mass is larger. The calculated residuals could serve as a quantitative index for evaluating the performance of the pseudo-static analysis to estimate the failure surface.

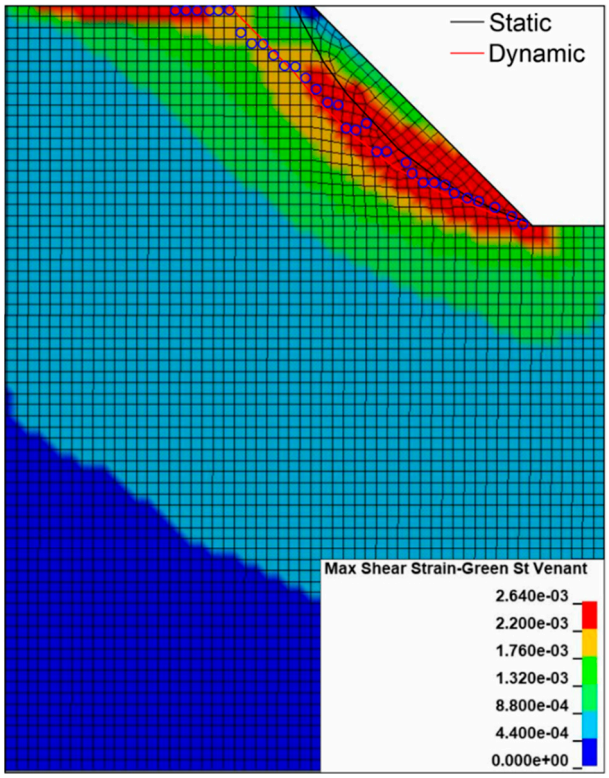

Figure 7. Determination of critical failure surface for Case 11 and Ofunato motion scaled to PGA = 0.25 g.

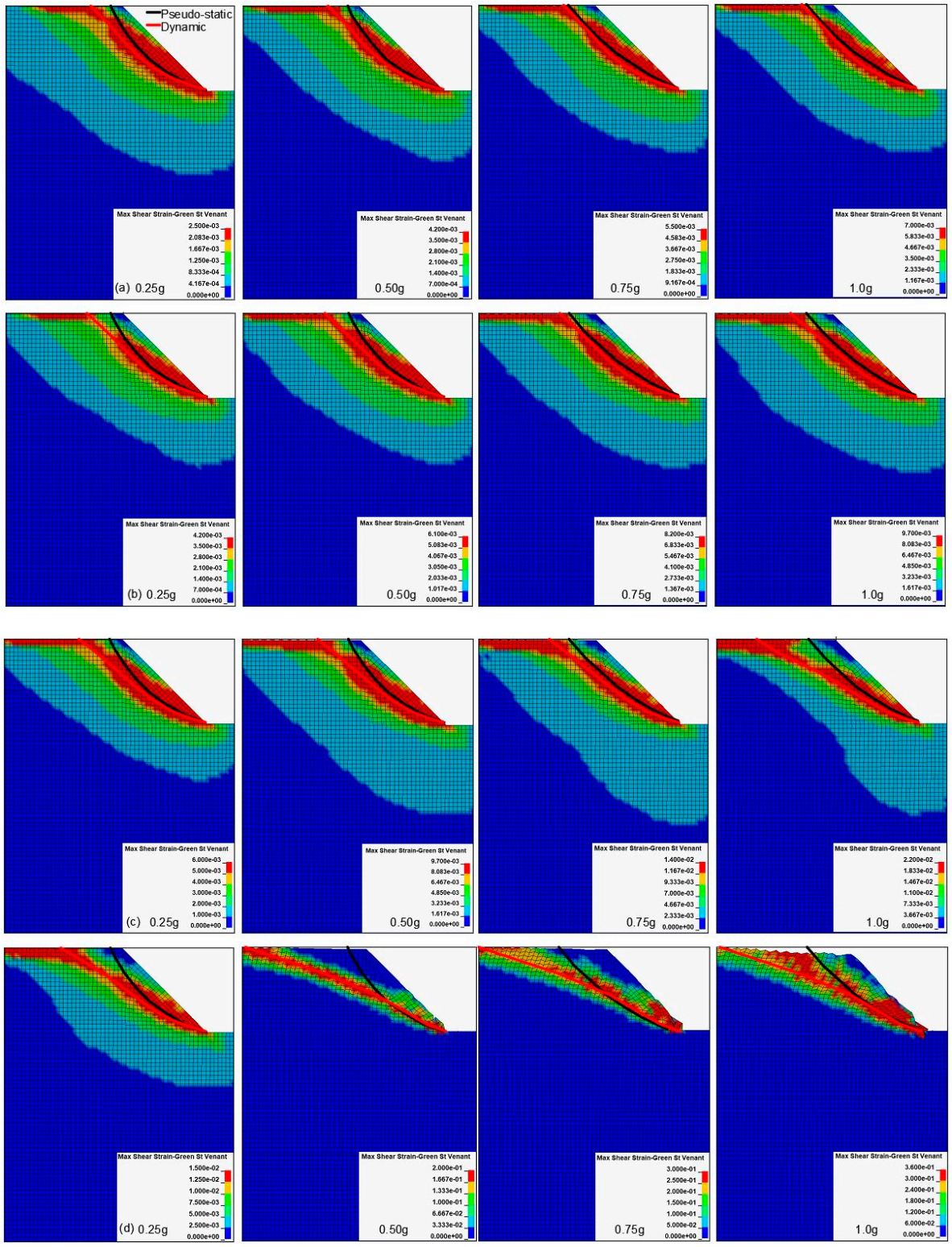

Figure 8. Effect of input motion on the slope failure surface for Case 09: (**a**) Whittier Narrows; (**b**) Northridge; (**c**) Ofunato; (**d**) Kobe.

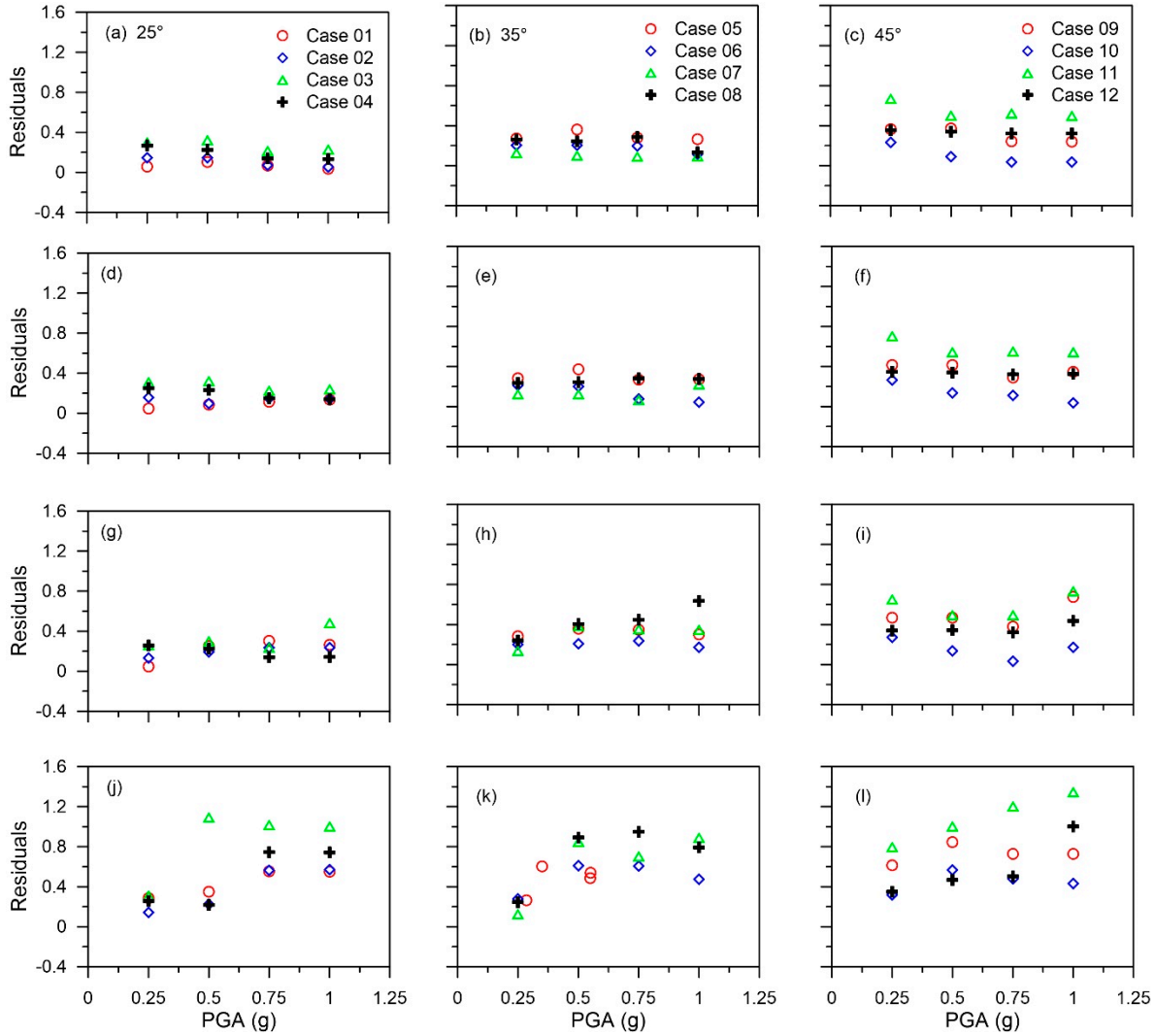

Figure 9. Residuals of failure surface: (**a**–**c**) Whittier Narrows (**d**–**f**) Northridge (**g**–**i**) Ofunato (**j**–**l**) Kobe.

For the Whittier Narrows and Northridge motions, the effect of the intensity is negligible for slopes inclined at 25° and 35°. The influence of the soil strength parameters is also not shown to be consistent. The range of residuals lies between 0 to 0.4. For the steepest slope with an inclination angle of 45°, both motions show a decreasing trend with an increase in the intensity. The cause for this characteristic is the widening of the pseudo-static-based surface with an increase in the intensity, as presented in the previous section. For the Ofunato motion, the trend is consistent with two motions with shorter mean periods for the slope angled at 25°. For the 35° slope angle, the residual increases with intensity for Case 8, for which the strength is the highest. It is considered that the stronger soil resists premature failure and produces wider sliding surface. For cases with lower strengths, the intensity is demonstrated to have marginal influence. For the slopes inclined at 45°, fluctuations in the outputs are observed. In general, the residuals tend to increase with intensity, although the influence is marginal. For the Kobe motion, the influence of the ground motion intensity is most clearly observed. An increase in the intensity of the ground motion causes a widening of the sliding surface, and corresponding increase in the residual. Even for slopes inclined at 25° and 35°, this pattern is well visible. The residuals are highest for the steepest slope. It should be noted that the trend of the residual with intensity is different for 45° slope. For the Whittier Narrows and Northridge motions, which have shorter mean periods, the residuals decrease with intensity. For the

Ofunato and Kobe motions, for which the mean periods are longer, the residuals increase with intensity, producing an inverse trend.

The comparisons highlight that for slopes with inclination angles less or equal to 35° subjected to motions with mean period shorter than 0.3 s, the residual between the sliding surfaces determined from a pseudo-static and dynamic analyses are not significant. However, for steep slopes and motions with a mean period of longer than 0.3 s, the residuals become non-negligible. For such cases, it is recommended to derive the failure surface directly from a dynamic analysis rather than a predefined surface calculated from a pseudo-static analysis.

5. Discussion

As noted in the introduction of this paper, the characterization of the failure surface is not only relevant to the pseudo-static analysis, but even to a dynamic analysis. It is because the stresses imposed along a predefined failure surface is integrated to determine Newmark sliding block displacement or dynamic factor of safety. The outputs of this study demonstrate that the failure surface is not only dependent on the slope and soil characterizations, in which case the predetermined failure surface can be used. Rather, it is also dependent on the frequency content and intensity of the input ground motion. Therefore, a predefined sliding surface should not be used in deriving the Newmark displacement or the dynamic factor of safety. The advantages of utilizing the finite element method to derive the failure surface were also documented in previous studies [31,32]. Crespellani et al. [33] also reported that the seismic displacement prediction is sensitive to the location of the failure surface.

A future study to characterize and quantify the influence of the Newmark displacement and dynamic factor of safety is warranted. The effect of the failure surface is estimated to strongly influence the outputs for regions of high seismicity, because the failure surface has a tendency to widen with the intensity and mean period of the input motion.

6. Conclusions

The objective of this study is to evaluate the sensitivity of the sliding surface to input motion intensity and frequency characteristics for a range of slope characterizations. A series of 2D nonlinear dynamic FE analyses is performed. The sliding surface is calculated from the contour of maximum shear strain at the end of shaking. The sliding surfaces determined from the dynamic analyses are extensively compared with those derived from pseudo-static analyses. The differences in the calculated sliding surfaces are quantified with the residual, which is defined as the discrepancy in the mobilized soil mass area above the surface in log normal unit. The following conclusions are drawn from the comparative results presented in this study:

- It is shown that the sliding surface may vary with the intensity and frequency characteristics of the input motion. Slopes with inclination angle equal or less than 35° are marginally influenced by the motion intensity if T_m < 0.3 s. For such cases, the residuals are less than 0.4. Slopes inclined at 45° are demonstrated to be more sensitive to the motion intensity and T_m.
- For motions with T_m < 0.3 s, the sliding surfaces determined from dynamic analyses are not highly influenced by the motion intensity. In contrast, the surface widens with intensity when calculated from a pseudo-static analysis. Because of these contrasting trends, the residual in the calculated sliding surfaces decreases with an increase in intensity.
- For motions with T_m > 0.3 s, the sliding surface derived from a dynamic analysis is demonstrated to widen with an increase in the intensity of the input ground motions. The degree of widening generally increases proportionally with an increase in T_m.
- It is, therefore, recommended to derive sliding surfaces from a dynamic analysis for steep slopes. It should, however, be noted that the conclusions are based on a limited

number of motions. Further studies are warranted to quantify the discrepancy in the calculated sliding surfaces using an extensive series of motions.

- It is recommended that, when determining the Newmark displacement or dynamic factor of safety from a dynamic analysis, the failure surface should be determined from the shear strain contour at the end of the simulation. This additional procedure is particularly relevant for the design of slopes in highly active regions, for which the use of a predefined surface determined from a limit equilibrium method is discouraged.

Author Contributions: M.I.K., Y.L. (Yonggook Lee), Y.-L. (Yonghee Lee), H.-S.K. and D.P. conceived the idea, outlined the work and co-wrote the manuscript; M.I.K. performed the numerical analyses and co-wrote the manuscript; Y.L. (Yonggook Lee) supported in performing the numerical simulations and summarizing the results. All authors have read and agreed to the published version of the manuscript.

Funding: This research was jointly supported by a project titled "Evaluation of the dynamic response of nuclear slopes through reduced model tests" funded by Korea Hydro & Nuclear Power Co. and by a grant (18SCIP-B146946-01) from the Construction Technology Research Program funded by Ministry of Land, Infrastructure and Transport of Korean government.

Institutional Review Board Statement: Not applicable.

Informed Consent Statement: Not applicable.

Data Availability Statement: Data sharing not applicable.

Conflicts of Interest: The authors declare no conflict of interest.

References

1. Keefer, D.K. Landslides caused by earthquakes. *Geol. Soc. Am. Bull.* **1984**, *95*, 406–421. [CrossRef]
2. Gorum, T.; Fan, X.; van Westen, C.J.; Huang, R.Q.; Xu, Q.; Tang, C.; Wang, G. Distribution pattern of earthquake-induced landslides triggered by the 12 May 2008 Wenchuan earthquake. *Geomorphology* **2011**, *133*, 152–167. [CrossRef]
3. Kramer, S.L. *Geotechnical Earthquake Engineering*; Prentice-Hall: Upper Saddle River, NJ, USA, 1996.
4. Baker, R.; Shukha, R.; Operstein, V.; Frydman, S. Stability charts for pseudo-static slope stability analysis. *Soil Dyn. Earthq. Eng.* **2006**, *26*, 813–823. [CrossRef]
5. Loáiciga, H.A. Groundwater and earthquakes: Screening analysis for slope stability. *Eng. Geol.* **2015**, *193*, 276–287. [CrossRef]
6. Newmark, N.M. Effects of earthquakes on dams and embankments. *Geotechnique* **1965**, *15*, 139–160. [CrossRef]
7. Jibson, R.W. Predicting earthquake-induced landslide displacements using Newmark's sliding block analysis. *Transp. Res. Rec.* **1993**, *1411*, 9–17.
8. Jibson, R.W. Regression models for estimating coseismic landslide displacement. *Eng. Geol.* **2007**, *91*, 209–218. [CrossRef]
9. Saygili, G.; Rathje, E.M. Empirical predictive models for earthquake-induced sliding displacements of slopes. *J. Geotech. Geoenviron.* **2008**, *134*, 790–803. [CrossRef]
10. Rathje, E.M.; Antonakos, G. A unified model for predicting earthquake-induced sliding displacements of rigid and flexible slopes. *Eng. Geol.* **2011**, *122*, 51–60. [CrossRef]
11. Tsai, C.-C.; Chien, Y.-C. A general model for predicting the earthquake-induced displacements of shallow and deep slope failures. *Eng. Geol.* **2016**, *206*, 50–59. [CrossRef]
12. Bouckovalas, G.D.; Papadimitriou, A.G. Numerical evaluation of slope topography effects on seismic ground motion. *Soil Dyn. Earthq. Eng.* **2005**, *25*, 547–558. [CrossRef]
13. Rizzitano, S.; Cascone, E.; Biondi, G. Coupling of topographic and stratigraphic effects on seismic response of slopes through 2D linear and equivalent linear analyses. *Soil Dyn. Earthq. Eng.* **2014**, *67*, 66–84. [CrossRef]
14. Luo, Y.; Fan, X.; Huang, R.; Wang, Y.; Yunus, A.P.; Havenith, H. Topographic and near-surface stratigraphic amplification of the seismic response of a mountain slope revealed by field monitoring and numerical simulations. *Eng. Geol.* **2020**, *271*, 105607. [CrossRef]
15. Lee, J.-H.; Ahn, J.-K.; Park, D. Prediction of seismic displacement of dry mountain slopes composed of a soft thin uniform layer. *Soil Dyn. Earthq. Eng.* **2015**, *79*, 5–16. [CrossRef]
16. Tsai, C.C.; Lin, C.H. Prediction of earthquake-induced slope displacements considering 2D topographic amplification and flexible sliding mass. *Soil Dyn. Earthq. Eng.* **2018**, *113*, 25–34. [CrossRef]
17. Fotopoulou, S.; Pitilakis, K. Predictive relationships for seismically induced slope displacements using numerical analysis results. *Bull. Earthq. Eng.* **2015**, *13*, 3207–3238. [CrossRef]
18. Cho, Y.; Rathje, E.M. Displacement hazard curves derived from slope-specific predictive models of earthquake-induced displacement. *Soil Dyn. Earthq. Eng.* **2020**, *138*, 106367. [CrossRef]

19. LSTC. *LS-DYNA Theory Manual*; Livermore Software Technology Corporation: Livermore, CA, USA, 2007.
20. Hashash, Y.; Musgrove, M.; Harmon, J.; Ilhan, O.; Groholski, D.; Phillips, C.; Park, D. *DEEPSOIL 7.0, User Manual*; University of Illinois at Urbana-Champaign: Springfield, IL, USA, 2017.
21. Hashash, Y.M.A.; Dashti, S.; Musgrove, M.; Gillis, K.; Walker, M.; Ellison, K.; Basarah, Y.I. Influence of Tall Buildings on Seismic Response of Shallow Underground Structures. *J. Geotech. Geoenviron.* **2018**, *144*, 04018097. [CrossRef]
22. Kuhlemeyer, R.L.; Lysmer, J. Finite element method accuracy for wave propagation problems. *J. Soil Mech. Found. Div.* **1973**, *99*, 421–427. [CrossRef]
23. Bolisetti, C. *Site Response, Soil-Structure Interaction and Structure-Soil-Structure Interaction for Performance Assessment of Buildings and Nuclear Structures*; 1321569084; State University of New York at Buffalo: Buffalo, NY, USA, 2015.
24. Bolisetti, C.; Whittaker, A.S.; Coleman, J.L. Linear and nonlinear soil-structure interaction analysis of buildings and safety-related nuclear structures. *Soil Dyn. Earthq. Eng.* **2018**, *107*, 218–233. [CrossRef]
25. Darendeli, M.B. Development of a New Family of Normalized Modulus Reduction and Material Damping Curves. Ph.D. Thesis, University of Texas at Austin, Austin, TX, USA, 2001.
26. Groholski, D.R.; Hashash, Y.M.A.; Kim, B.; Musgrove, M.; Harmon, J.; Stewart, J.P. Simplified Model for Small-Strain Nonlinearity and Strength in 1D Seismic Site Response Analysis. *J. Geotech. Geoenviron.* **2016**, *142*, 04016042. [CrossRef]
27. Motamed, R.; Stanton, K.; Almufti, I.; Ellison, K.; Willford, M. Improved approach for modeling nonlinear site response of highly strained soils: Case study of the service hall array in Japan. *Earthq. Spectra* **2016**, *32*, 1055–1074. [CrossRef]
28. Lee, Y.; Kim, H.-S.; Khalid, M.I.; Lee, Y.; Park, D. Effect of Nonlinear Soil Model on Seismic Response of Slopes Composed of Granular Soil. *Adv. Civ.* **2020**, *2020*, 8890247.
29. Yoo, J.-K.; Park, D.; Baxter, C.D. Estimation of drained shear strength of granular soil from shear wave velocity and confining stress. *J. Geotech. Geoenviron.* **2018**, *144*, 04018027. [CrossRef]
30. SLOPE/W. *GEO-SLOPE International*; SLOPE/W: Calgary, AB, Canada, 2018.
31. Li, X. Finite element analysis of slope stability using a nonlinear failure criterion. *Comput. Geotech.* **2007**, *34*, 127–136. [CrossRef]
32. Griffiths, D.; Fenton, G.A. Probabilistic slope stability analysis by finite elements. *J. Geotech. Geoenviron.* **2004**, *130*, 507–518. [CrossRef]
33. Crespellani, T.; Madiai, C.; Vannucchi, G. Earthquake destructiveness potential factor and slope stability. *Geotechnique* **1998**, *48*, 411–419. [CrossRef]